How coherent are Josephson junctions?

Hanhee Paik,[1] D. I. Schuster,[1,2] Lev S. Bishop,[1,3] G. Kirchmair,[1] G. Catelani,[1]
A. P. Sears,[1] B. R. Johnson,[1,4] M. J. Reagor,[1] L. Frunzio,[1] L. Glazman,[1] and R. J. Schoelkopf[1]

[1]*Department of Physics and Applied Physics, Yale University, New Haven, Connecticut 06520, USA*
[2]*Department of Physics and James Franck Institute, University of Chicago, Chicago, Illinois 60637, USA*
[3]*Joint Quantum Institute and Condensed Matter Theory Center, Department of Physics, University of Maryland, College Park, Maryland 20742, USA*
[4]*Raytheon BBN Technologies, Cambridge, MA 02138, USA*

(Dated: May 26, 2011)

Attaining sufficient coherence is a requirement for realizing a large-scale quantum computer. We present a new implementation of a superconducting transmon qubit that is strongly coupled to a three-dimensional superconducting cavity. We observe a reproducible increase in the coherence times of qubit (both T_1 and $T_2 > 10\ \mu$s) and cavity ($T_{\rm cav} \sim 50\ \mu$s) by more than an order of magnitude compared to the current state-of-art superconducting qubits. This enables the study of the stability and quality of Josephson junctions at precisions exceeding one part per million. Surprisingly, we see no evidence for $1/f$ critical current noise. At elevated temperatures, we observe the dissipation due to a small density ($< 1-10$ ppm) of thermally-excited quasiparticles. The results suggest that the overall quality of Josephson junctions will allow error rates of a few 10^{-4}, approaching the error correction threshold.

PACS numbers: 42.50.Pq, 03.67.Lx, 85.25.-j

Superconducting circuits are a promising technology for quantum information processing with solid-state devices. Several different types of qubits [1, 2] have been developed, which all rely on the nonlinearity of one or more Josephson junctions. Ideally, the Josephson junctions should be dissipationless and highly stable to avoid decoherence, while providing the crucial anharmonicity that allows individual energy levels to be separately addressed. Although the coherence time of superconducting qubits has increased about three orders of magnitude in the past decade, from initially only a few nanoseconds to typically about a microsecond today, it is still not clear if there are fundamental limits imposed by the junctions. Since one and two-qubit operations require tens of nanoseconds, the current coherence times allow operations to be performed with error rates on the order of one percent [3, 4]. This has permitted experiments where multiple qubits are controlled, entangled [5–8], and used to demonstrate simple algorithms [9]. However, a major outstanding question is whether qubit coherence can further improve by the one or two orders of magnitude necessary to reach the level for practical quantum error correction [10].

The coherence of a qubit can either be limited by possible imperfections in the Josephson junctions, or by unintended interactions with the environment. Even if the junctions were perfectly coherent, achieving a long coherence time also requires understanding and controlling the Hamiltonian such that the terms coupling the qubit to the outside world can be made small. For example, in the hydrogen atom a coupling of only 40 ppb to the electromagnetic continuum gives rise to spontaneous emission and a quality factor, Q, of about 25 million. Building a scalable quantum computer using superconducting qubits therefore requires engineering a Hamiltonian where the undesirable couplings that lead to decoherence are kept at the part per million to part per billion level. So can a manmade, macroscopic quantum system based on Josephson junctions have well-defined quantum states that approach this level of coherence?

Here we present results on a new implementation of a superconducting qubit where we carefully control the coupling to the environment, obtaining an increase in coherence by over an order of magnitude. We observe reproducible qubit lifetimes for relaxation (T_1) up to 60 μs, and lifetimes of coherent superpositions (T_2) of 15 - 20 μs, corresponding to quality factors for both dissipation ($Q_1 = \omega_{01} T_1 \sim 2\times10^6$, where ω_{01} is the transition frequency of the qubit) and decoherence ($Q_2 = \omega_{01} T_2 \sim 7\times10^5$) of about one million. The high quality factors observed imply that the instability in the parameters of our system, the intrinsic dissipation in the Josephson junction, and the size of the undesired couplings are all in fact smaller than one part per million. These results also suggest that existing Josephson junction technology should allow superconducting circuits to achieve coherence levels compatible with scalable quantum computing in the solid state.

Our experiment employs a particularly simple transmon qubit [13, 24], consisting of just two superconducting electrodes connected with a single small aluminum Josephson junction, that requires no bias circuitry and has minimal sensitivity to $1/f$ noises in charge or flux, coupled to a microwave resonant cavity that can act as an entanglement bus and readout circuit. Neglecting the interactions with its environment, the transmon is described by the simple Hamiltonian [12, 13],

$$\hat{H} = 4E_C(\hat{n}-n_0)^2 - E_J\cos\hat{\phi} \qquad (1)$$

where $\hat{n}$ and $\hat{\phi}$ are the normalized operators for the pair charge and phase (obeying $[\hat{\phi},\hat{n}] = i$), $E_J = \hbar I_c/2e$ and $E_C = e^2/2C_\Sigma$ are the Josephson and Coulomb energies, e is the electron's charge, I_c is the junction critical current, C_Σ is the total capacitance between the electrodes, and n_0 is the charge offset.

The experiments are performed using a circuit QED architecture [11, 19] to isolate, couple, and measure the qubit. A novel aspect is the use of a three-dimensional waveguide cavity machined from superconducting aluminum (alloy 6061

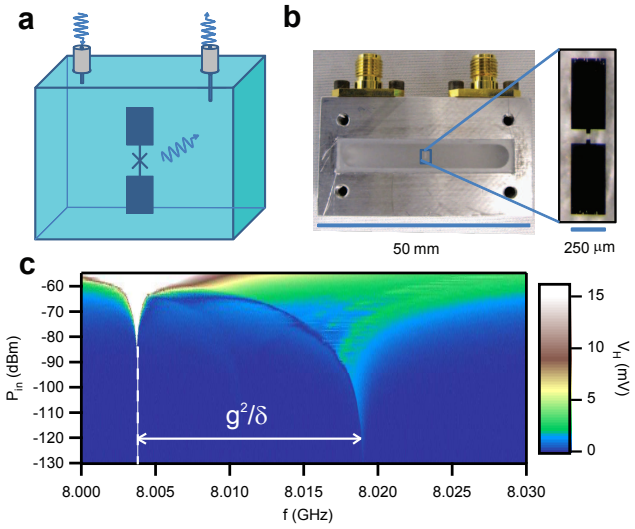

FIG. 1: Qubit coupled to a 3D cavity (a) Schematic of a transmon qubit inside a 3D cavity. The qubit is coupled to the cavity through a broadband dipole antenna that is used to receive and emit photons. (b) Photograph of a half of the 3D aluminum waveguide cavity. An aluminum transmon qubit with the the dipole antenna is fabricated on a c-plane sapphire substrate and is mounted at the center of the cavity. (Inset) Optical microscope image of a single-junction transmon qubit. The dipole antenna is 1 mm long. (c) Transmission of a 3D cavity (cavity D) coupled to a transmon ($J1$) measured as a function of power and frequency. The cavity response above -80 dBm occurs at the bare cavity frequency f_c = 8.003 GHz. At lower powers, the cavity frequency shifts by g^2/δ.

T6, see supplement for details), as shown in Fig. 1a-1b. This type of cavity offers several advantages over the planar transmission-line cavities used in previous circuit QED experiments [11, 14, 15]. First, the cavity has a larger mode volume (approximately 3 cm^3 or one tenth of a cubic wavelength, compared to the 10^{-6} cubic wavelengths for a conventional transmission line resonator), and is much less sensitive to the surface dielectric losses that are suspected as the limiting source of dissipation in transmission line resonators to date [16, 17]. Indeed, we have observed reproducible quality factors of these cavities [18] of 2 to 5 million, corresponding to photon storage times in excess of 50 μs (not shown) in the quantum regime ($k_BT \ll \hbar\omega_c$ and $\langle n\rangle \sim 1$, where ω_c is the cavity frequency), without the power dependence [16, 17] indicative of the presence of two-level systems. Second, the geometry presents the qubit with a well-controlled electromagnetic environment, limiting the possibility of relaxation through spontaneous emission into the multiple modes that may be possible with a complicated chip and its associated wiring [15]. The qubit is placed in the center of the cavity, maximizing the coupling to the lowest frequency TE101 mode at $\omega_c/2\pi \sim 8$ GHz, which is used for readout and control. This location also nulls the coupling to the second mode (TE102 at approximately 12 GHz).

Despite the larger mode volume of the three-dimensional cavity, we are able to achieve the strong-coupling limit of cavity QED in this system, with vacuum Rabi frequencies, $g/2\pi$, greater than 100 MHz. As seen in Figure 1b, the electrodes of the qubit are significantly larger (~ 0.5 mm) than in a conventional transmon qubit, so that the increased dipole moment of the qubit compensates for the reduced electric field that a single photon creates in the cavity. We note that due to the large dipole moment, the expected lifetime from spontaneous emission in free space would be only of ~ 100 ns, so that a high-Q cavity is required to maintain the qubit lifetime. The electrodes also form the shunting capacitance ($C_\Sigma \sim 70$ fF) of the transmon, giving it the same anharmonicity and the same insensitivity to $1/f$ charge noise as in the conventional design. An advantage of this qubit design is that the large electrode size reduces the sensitivity of the qubit to surface dielectric losses, which may be responsible for the improved relaxation times. Because in this experiment the qubits cannot be tuned into resonance with the cavity, the vacuum Rabi coupling is not observed directly. The system is rather operated in the dispersive limit ($|\delta| = |\omega_c - \omega_{01}| \gg g$) [19]. Here the qubit induces a state-dependent shift, χ, on the cavity, which is the basis of the readout mechanism. The dispersive shifts are typically several tens of MHz (see Table 1), and can approach 1,000 times the linewidths of qubit and cavity, so that all devices are well within the strong dispersive limit [14]. The transmission through the cavity as a function of microwave power, which demonstrates the ground-state shift of the cavity and the re-emergence of the bare cavity frequency at sufficiently high powers (see Ref.[20, 21]) is shown in Figure 1c. Single-shot readout of the qubit (with fidelities greater than 70%) is performed using the technique previously described [20].

To investigate the Hamiltonian of the qubit and its properties, we perform spectroscopy by exciting the qubit transition with microwave signals coupled off-resonantly through the cavity, followed by a readout pulse lasting a few microseconds. Experiments are performed in a cryogen-free dilution refrigerator at 10 mK. The spectrum obtained on a wide scale is shown in Figure 2a, and it displays the expected frequency difference between subsequent excitations, or anharmonicity ($\alpha/2\pi = f_{12} - f_{01} \sim -200$ MHz to -300 MHz). This anharmonicity is very similar to that of the conventional transmon design, allowing fast single-qubit operations in ~ 20 ns (see Supplement). An examination of the lineshape for the transition between ground and first excited state as a function of the drive power is shown in Fig. 2b. The high degree of coherence is demonstrated by the narrow linewidths. The minimum values observed (Fig. 2c) for Δf_{HWHM} are about 10 kHz, corresponding to a coherence time $T_2 = (2\pi\Delta f_{HWHM})^{-1} = 16$ μs.

The dramatically improved coherence properties of these qubits are confirmed via the standard time-domain measurements of the relaxation time (T_1) and Ramsey experiments (T_2) (see Figure 3 and Table 1). There are several surprising features. First, while T_2's are typically in the range of 15 - 20 μs, they do not yet attain the limit twice T_1; the latter is reproducibly in the range 25 - 50 μs corresponding to Q_1= 1 - 2$\times 10^6$. This indicates that there is still significant dephasing. At the same time, both the Ramsey decay envelope and the echo coherence (which has an artificial phase rotation as a function of the delay added) can be fit well by

qubit (*cavity*)	f_{01} (GHz)	E_J (GHz)	E_C (GHz)	$g/2\pi$ (MHz)	$g^2/2\pi\delta$ (MHz)	f_c (GHz)	Q_c ($x10^3$)	T_1 (μs)	T_2 (μs)	$T_{\rm echo}$ (μs)
J1 (D)	6.808	21.1	0.301	138	15.9	8.0035	340	60	18	25
J1a (D)	6.769	21.0	0.301	140	15.8	8.00375	340	50	20	24
J2 (C)	7.772	28.6	0.292	152	99.8	8.0020	360	25	15	21
J3 (B)	7.058	22.5	0.304	141	21.5	7.9835	320	42	12	12
S (D)	7.625	34.4	0.227	136	48.2	8.01065	340	35	7.3	11
Sa (A)	7.43	32.5	0.228	123	24.1	8.06169	100	20	6	8

TABLE I: Parameters of four transmon qubits (labeled as J's for single-junction qubits and S's for SQUID) measured in four different 3D cavities (labeled as A, B, C and D respectively). The data of $J1a$ and Sa are data on qubits J1 and S following cycling to room temperature. Here, $f_{01} = \omega_{01}/2\pi$ is the dressed qubit transition frequency between ground state $|0\rangle$ and the first excited state $|1\rangle$, $g/2\pi$ is the coupling strength, $g^2/2\pi\delta$ is the cavity frequency shift from the bare cavity frequency due to the qubit, $f_c = \omega_c/2\pi$ is the bare cavity frequency, cavity Q_c is the quality factor of the χ-shifted cavity resonance at single-photon power, T_1 is the relaxation time from $|1\rangle$ to $|0\rangle$, T_2 is the coherence time measured by Ramsey experiment, and $T_{\rm echo}$ is the coherence time measured by spin-echo experiment.

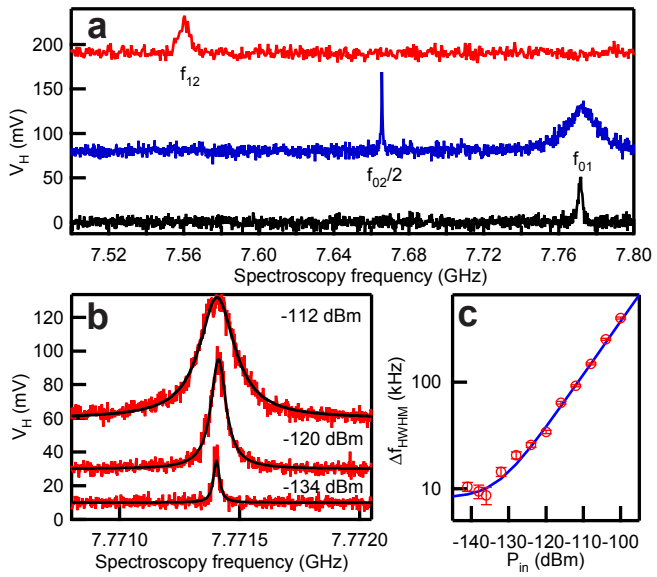

FIG. 2: Qubit spectroscopy (a) Spectrum of qubit $J2$ showing anharmonic energy levels where f_{12} is the transition frequency between the first excited state $|1\rangle$ and second excited state $|2\rangle$, $f_{02}/2$ is the two photon transition frequency between the ground state $|0\rangle$ and $|2\rangle$ and f_{01} is between $|0\rangle$ and $|1\rangle$. Transition f_{12} was measured with two microwave sources where one excites f_{01} and the other scans for f_{12}. (b) The resonance peak of f_{01} versus power from qubit $J2$ (c) Spectroscopic half-width-half-maximum (HWHM) linewidth versus driving power. Blue curve shows a theoretical power dependence of Δ_{HWHM} from the driven two-level system model, as described in Ref. [22].

an exponential decay, indicating that $1/f$ noise is essentially absent. This is consistent with the expectation that these simple qubits should avoid dephasing due to both $1/f$ flux noise (since there are no superconducting loops) and charge noise (since the total charge variation of the transition frequency [13] for these transmon parameters is less than 1 kHz). The observed phase coherence factor, $Q_2 \sim 700,000$, is an order of magnitude larger than previous superconducting devices [23, 24]. Since the transition frequency of the transmon qubit ($\omega_{01} \sim \sqrt{8E_JE_C}$) is set by a combination of the Josephson and charging energies, this allows us to place stringent limits on the amount of critical current noise in Josephson junctions, or dielectric fluctuations in the shunt capacitance. We find that any critical current noise must have a total variance of less than about one part per million ($\delta I/I_c < 10^{-6}$), even smaller than the $1/f$ contribution predicted by scaling both the junction area and operating temperature as suggested in previous studies of critical current noise in SQUIDs [25, 27]. In fact, the observed Ramsey and echo decays are more consistent with frequency-independent noise in the qubit transition frequency (or critical current) of about $\sqrt{S_{\omega/\omega_{01}}} \sim 10$ ppb$/\sqrt{\rm Hz}$ or $\sqrt{S_{I/I_c}} \sim 20$ ppb$/\sqrt{\rm Hz}$. The improvement by approximately a factor of two with echo indicates either a characteristic correlation time in this noise of about 10 μs, or an additional low-frequency noise (but not $1/f$ in character) component with a variance of about 1 ppm.

The high stability of the qubit transition frequency is exhibited in Fig. 3c, which shows the deviations observed in the Ramsey detuning compared to the microwave generator over one day. The parameters in the Hamiltonian of this artificial quantum system are seen to be stable for long periods to within ~ 600 Hz or ~ 80 parts per billion over many hours. Discrete jumps of a few kHz (or about 1 part per million) are occasionally observed, and are consistent in size with that expected by single atomic rearrangements in the tunnel junction barrier. On subsequent thermal cycling of two devices, a slow telegraph switching behavior (with $\delta f \sim 5-50$ kHz) was also observed. These observations confirm the ability of this type of experiment to reveal tiny variations in junction parameters which would be undetectable in previous superconducting qubit experiments.

It is still not clear what mechanisms limit the coherence in these new qubits, but some information can be obtained by measuring the dependence of coherence times on sample temperature, as shown in Figure 4. The most striking effect is the rapid decrease in the relaxation time, T_1, once the temperature exceeds about 130 mK, which is in good quantitative agreement with a recent theory on the effects of quasiparticles [26], using only a single fit parameter which is the gap of the superconductor (Δ = 194 μeV). The saturation of the relaxation times below this temperature means that either the qubits are limited by the presence of out-of-equilibrium quasiparticles, or other mechanisms such as spontaneous emission

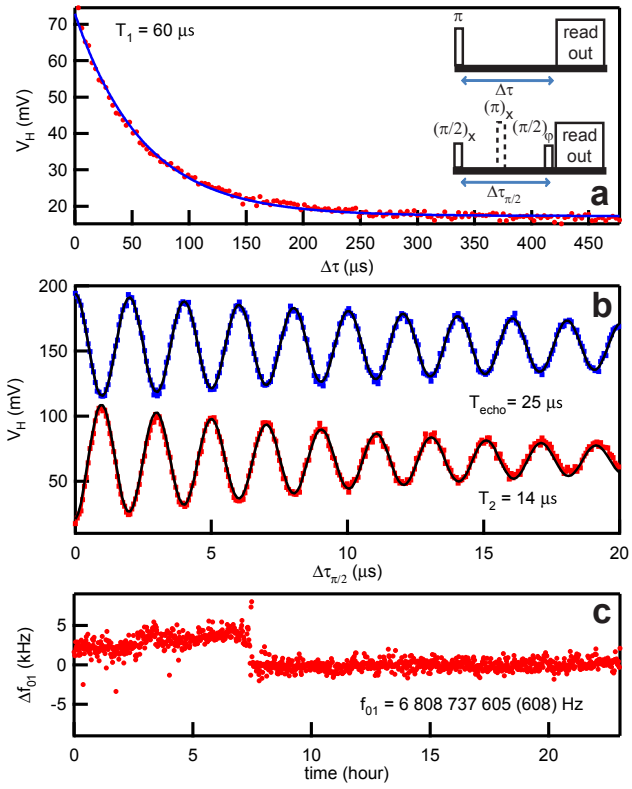

FIG. 3: Time domain measurement of the qubit coherence (a) Relaxation from $|1\rangle$ of qubit $J1$. T_1 is 60 μs for this measurement. (Inset) The pulse sequences used to measure relaxation (upper) and Ramsey experiments with and without echo (lower). The pulse shown in dashed line is an echo signal applied at one half of the delay between two $\pi/2$ pulses. (b) Ramsey fringes measured on resonance with (blue squares) and without (red squares) echo sequence. The pulse width for the π and $\pi/2$ pulses used in the experiments is 20 ns. An additional phase is added to the rotation axis of the second $\pi/2$ pulse for each delay to give the oscillatory feature to the Ramsey fringes. (c) Qubit frequency f_{01} measured over 23 hours by repeated Ramsey measurements.

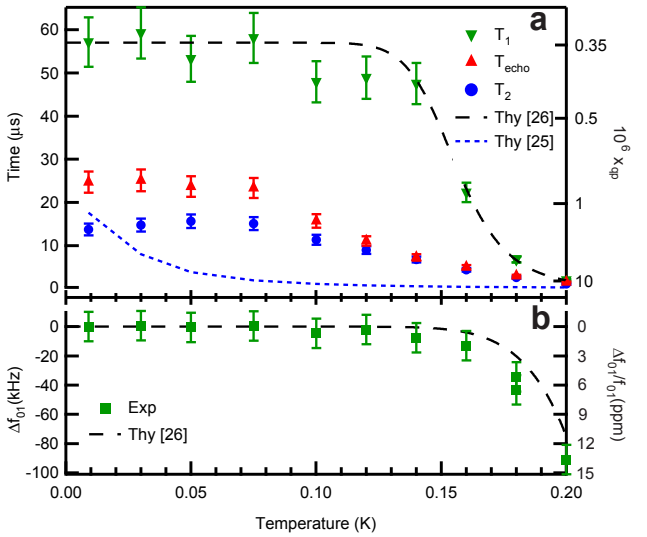

FIG. 4: Temperature dependence of qubit properties (a) Measurement of T_1, $T_{\rm echo}$ and T_2 (b) Shift of the transition frequency f_{01}. Black dashed curves in (a) and (b) are theoretical T_1 and f_{01} calculated from the model in Ref.[26] plus a temperature-independent relaxation rate with the same fitting parameter of Δ = 194 μeV for both T_1 and f_{01} (See supplement for details). Blue dashed curve is the theoretical T_2 from $1/f$ critical current fluctuations predicted by Ref.[25]

(the Purcell effect) or dielectric losses in the sapphire. The observed times place a stringent upper bound on the density of these quasiparticles, which is less than one quasiparticle per cubic micron, or or a normalized quasiparticle density ($x_{qp} = n_{qp}/n_{pairs} < 5 \times 10^{-7}$ where n_{qp} is the density of quasiparticles and n_{pairs} is the density of Cooper pairs). This is an order of magnitude lower density than reported in recent measurements on phase qubits [28] or transmission-line resonators[29]. We also observe (lower panel) a frequency shift of the qubit transition due to the induced thermal quasiparticles, again in quantitative agreement with the predictions of Reference [26]. The decoherence times T_2 and $T_{\rm echo}$ are observed to decrease slowly with temperature, inconsistent with either the quadratic [25] or linear [27] temperature scalings reported previously for critical current noise. Another mechanism for relaxation is spontaneous emission of the qubit via the cavity (the Purcell effect), which is consistent with the general trend that qubits with smaller detunings from the cavity tend to have shorter lifetimes. Our estimates of the multimode Purcell effect [15] for these cavities predict only a small contribution to T_1 for most devices measured so far, but the data do not yet allow a detailed test of the Purcell model. Further experiments which vary qubit and cavity parameters will be required to identify and hopefully further reduce decoherence. Nonetheless, the current results already indicate that the intrinsic quality factor of Josephson junctions is greater than one million.

It is quite remarkable that a macroscopic, manmade device such as a superconducting qubit can be so coherent. For instance, the simple Hamiltonian given in Eq. (1) is analogous in complexity and sophistication to a description of a hydrogen atom only by a combination of the Coulomb potential and a kinetic energy term, neglecting internal degrees of freedom such as spin or the interaction with the environment. In hydrogen, more subtle effects such as the coupling to the electromagnetic continuum and the hyperfine and fine structure already introduce line broadening or splittings at the level of 0.1 to 10 parts per million. The extreme stability and long coherence times obtained for superconducting qubits in this work allow us to rule out modifications from any low-energy degrees of freedom at the level of a fraction of only part per million. These results are therefore encouraging for all experiments with superconducting quantum circuits, and should probably allow future devices to approach the error levels required to satisfy the quantum error correction threshold.

We have presented a new implementation of superconducting qubits coupled to a microwave cavity and reproducibly obtained coherence times in excess of 10 μs, an improvement

of more than an order of magnitude over the current state-of-art. These qubits demonstrate remarkable long-term stability, indicating that critical current fluctuations are much smaller than previously predicted. The dissipation and the frequency shift as a function of temperature confirm recent theoretical predictions on the effects of thermally-induced quasiparticles. The lifetimes at low temperatures imply that the intrinsic quality factor of Josephson junctions can be greater than one million, and enable us to place significantly more stringent limits on any possible background density of non-equilibrium quasiparticles. The improved coherence was achieved without reducing either the anharmonicity or the coupling strength between the qubit and cavity, and should still allow fast one and two-qubit operations. Future experiments will seek to couple multiple qubits, which should allow operation of simple processors at significantly improved error rates.

We thank Michel Devoret, Steve Girvin, Eran Ginossar, Matt Reed, Leo DiCarlo, Luyan Sun and Shyam Shankar for valuable discussions. L. F. acknowledges partial support from CNR-Istituto di Cibernetica. This research was funded by the Office of the Director of National Intelligence (ODNI), Intelligence Advanced Research Projects Activity (IARPA), through the Army Research Office. All statements of fact, opinion or conclusions contained herein are those of the authors and should not be construed as representing the official views or policies of IARPA, the ODNI, or the U.S. Government.

[1] J. Clarke and F. K. Wilhelm, *Nature* **453**, 1031-1042 (2008)
[2] R. J. Schoelkopf and S. M. Girvin, *Nature* **451**, 664-669 (2008)
[3] J. Chow *et al.*, Phys. Rev. A **82**, 040305(R) (2010)
[4] E. Lucero *et al.*, Phys. Rev. A **82**, 042339 (2010)
[5] J. M. Chow *et al.*, Phys. Rev. A **81**, 062325 (2010)
[6] M. Ansmann *et al.*, Nature **461**, 504-506 (2009)
[7] L. DiCarlo *et al.* Nature **467** 574-578 (2010)
[8] M. Neeley *et al.* Nature **467** 570-573 (2010)
[9] L. DiCarlo *et al.* Nature **460** 240-244 (2009)
[10] J. Preskill, Proc. Roy. Soc. Lond. **A454**, 385-410 (1998)
[11] A. Wallraff *et al.*, Nature **431**, 162-167 (2004)
[12] M. H. Devoret and J. M. Martinis, *Quant. Info. Proc.* **3**, 163-203 (2004)
[13] J. Koch *et al.*, Phys. Rev. A **76**, 042319 (2007)
[14] D. I. Schuster *et al.*, Nature **445**, 515-518 (2007)
[15] A. A. Houck *et al.*, Phys. Rev. Lett. **101**, 080502 (2008)
[16] J. Gao *et al.*, Appl. Phys. Lett. **92**, 152505 (2008)
[17] A. D. O'Connell *et al.*, Appl. Phys. Lett. **92**, 112903 (2008)
[18] Paik *et al.*, manuscript in preparation (2011)
[19] A. Blais *et al.*, Phys. Rev. A **69**, 062320 (2004)
[20] M. D. Reed *et al.*, Phys. Rev. Lett. **105**, 173601 (2010)
[21] L. S. Bishop, E. Ginossar, S. M. Girvin, Phys. Rev. Lett. **105**, 100505 (2010)
[22] D. I. Schuster *et al.*, Phys. Rev. Lett. **94**, 123602 (2005)
[23] D. Vion *et al.*, Science **296**, 886-889 (2002)
[24] J. A. Schreier *et al.*, Phys. Rev. B **77**, 180502(R) (2008)
[25] D. J. Van Harlingen *et al.*, Phys. Rev. B **70**, 064517 (2004)
[26] G. Catelani *et al.*, Phys. Rev. Lett. **106**, 077002 (2011)
[27] J. Eroms *et al.*, Appl. Phys. Lett. **89**, 122516 (2006)
[28] M. Lenander *et al.*, arXiv:1101.0862v1 (2011)
[29] P. J. de Visser *et al.*, Phys. Rev. Lett. **106**, 167004 (2011)

Supporting Online Material for

How coherent are Josephson Junctions?

Hanhee Paik, D. I. Schuster, Lev S. Bishop, G. Kirchmair, G. Catelani,
A. P. Sears, B. R. Johnson, M. J. Reagor, L. Frunzio, L. Glazman, R. J. Schoelkopf

Materials and Methods

Qubit and antenna design and fabrication

Four qubits, J1, J2, J3 and S, are discussed in the paper. J1, J2 and J3 have a single Josephson junction with the area of 130×250 nm^2 (length × width) connected to a dipole antenna by 25 μm long and 1 μm wide aluminum wire. The dimensions of each arm of the antenna are 500×250 μm^2. S has two 130×130 nm^2 Josephson junctions in parallel in an 8×4 μm^2 SQUID loop configuration connected to a T-shaped dipole antenna. The horizontal arm of the T-shaped antenna is a 700 μm long and 25 μm wide aluminum wire with a 250×250 μm^2 pad attached to each end of it. The center of this arm is connected to one side of the SQUID loop. The other side is connected to the upper end of the vertical arm of the antenna, which is a 700 μm long and 25 μm wide aluminum wire with a 250×250 μm^2 pad attached to its lower end.

Josephson junctions and dipole antennas are fabricated in one single fabrication step, in a similar way as all of our previous transmons (1-6), by electron-beam lithography followed by aluminum double-angle electron-beam evaporation. The two evaporations deposit thin Al films with thickness of 20 nm and 60 nm respectively. The two layers are separated by an AlO_x barrier grown by thermal oxidation for 720 seconds in 2000 Pa static pressure of a gas mixture of 85% Argon and 15% Oxygen.

Cavity design and fabrication

Each microwave cavity is machined out of two blocks of 6061 aluminum alloy with $T_c \sim 1.5$ K. The outer dimensions of each aluminum block are $45.7 \times 25.4 \times 12.7$ mm^3 (length × width × height) and the cavity volume is $35.6 \times 5.1 \times 17.8$ mm^3. The cavity is excited and measured through capacitive pin couplers attached to SMA connectors.

Measurement setup

The state of the qubit is probed by measuring the qubit-state dependent cavity transmission using heterodyne detection. Figure S1 is a block diagram of the measurement setup. Microwave signals for control and measurement transmit through a coax with a 20 dB attenuator at 4 K and a -20 dB directional coupler followed by a 10 dB attenuator at 10 mK. The cavity transmission at the output goes through two cryogenic isolators at 10 mK and is amplified by a HEMT amplifier with a noise temperature of ~ 5 K at the 4 K stage. At room temperature, the transmission signal from the cavity is further amplified by two low-noise room temperature amplifiers and is mixed down to 10 MHz IF frequency with an IQ mixer.

Temperature dependence of T_1 and frequency shift due to quasiparticles

The temperature-dependence of the relaxation time T_1 and the frequency shift Δf_{01} in Fig. 4 in the main text can be ascribed to quasiparticles. Here we describe briefly an extension of the results for quasiparticle-induced relaxation and frequency shift of Ref. (7), whose details will be presented elsewhere (8). We assume that the quasiparticle distribution function $f(\varepsilon)$ is given by the sum of a temperature-independent, non-equilibrium part, $f_{ne}(\varepsilon)$, and a thermal equilibrium part, $f_{eq}(\varepsilon)$:

$$f(\varepsilon) = f_{ne}(\varepsilon) + f_{eq}(\varepsilon) \tag{1}$$

For the non-equilibrium term, we assume that the characteristic quasiparticle energy δE (as measured from the gap) is small compared to the qubit frequency, $\delta E << \hbar\omega$. For the thermal equilibrium contribution, we take the temperature small compared to the gap, $k_B T \ll \Delta$, so that $f_{eq}(\varepsilon)$ follows the Boltzmann distribution, but we make no assumptions on the ratio $k_B T / \hbar\omega$. The inverse quality factor is given by

$$\frac{1}{Q} = \frac{\Gamma_{1\to 0} + \Gamma_{0\to 1}}{\omega} \tag{2}$$

where $\Gamma_{1\to 0}$ and $\Gamma_{0\to 1}$ are quasiparticle-induced transition rates between the qubit states (7). With our assumptions, the non-equilibrium quasiparticles do not contribute to the upward $0\to 1$ transition rate, so that $\Gamma_{0\to 1} = \Gamma_{eq,0\to 1}$, while both non-equilibrium and equilibrium parts contribute to the downward rate, $\Gamma_{1\to 0} = \Gamma_{ne,1\to 0} + \Gamma_{eq,1\to 0}$. In agreement with detailed balance, the thermal equilibrium rates are related by $\Gamma_{eq,0\to 1} / \Gamma_{eq,1\to 0} = e^{-\hbar\omega/k_B T}$. The inverse quality factor takes the form

$$\frac{1}{Q} = \frac{x_{ne}}{\pi}\sqrt{\frac{2\Delta}{\hbar\omega}} + \frac{2}{\pi} e^{-\Delta/k_B T} e^{-\hbar\omega/2k_B T} K_0\left(\frac{\hbar\omega}{2k_B T}\right)\left[1 + e^{-\hbar\omega/k_B T}\right] = \frac{1}{\omega T_1} \tag{3}$$

where x_{ne} is the normalized density of non-equilibrium quasiparticles, K_0 is the modified Bessel function of the second kind, and Δ is the gap in the absence of quasiparticles. The data of the relaxation time T_1 in Fig. 4a are fit to Eq. (3) with two fitting parameters, the gap Δ = 194 μV and the normalized non-equilibrium density $x_{ne} = 4\times 10^{-7}$. At low temperatures, $k_B T \ll \hbar\omega$, this expression becomes

$$\frac{1}{Q} = \frac{x_{qp}}{\pi}\sqrt{\frac{2\Delta}{\hbar\omega}} \tag{4}$$

where $x_{qp} = x_{ne} + x_{eq}$ and

$$x_{eq} = \sqrt{\frac{2\pi k_B T}{\Delta}} e^{-\Delta/k_B T} \tag{5}$$

is the normalized equilibrium quasiparticle density. Equation (4) has been used to estimate the normalized quasiparticle density x_{qp} as indicated in the left scale in Fig.4a.

Under the same assumptions, the temperature dependence of the relative frequency shift is given by

$$\frac{\Delta f_{01}(T)}{f_{01}} = -\frac{2}{\pi} e^{-\Delta/k_B T} e^{-\hbar\omega/2k_B T} I_0\left(\frac{\hbar\omega}{2k_B T}\right) - \frac{x_{eq}}{2} \qquad (6)$$

with I_0 the modified Bessel function of the first kind. Note that since only the temperature dependence of the frequency can be measured, we can neglect the temperature-independent shift due to non-equilibrium quasiparticles. The theoretical curve in Fig. 4b is given by Eq. (6) using the value of the gap, $\Delta = 194$ μV, obtained from the fit for T_1.

Measurement of Rabi frequency as a function of power

The measurements of the time-domain Rabi oscillations as a function of power were performed using the flat-top pulses with rise and fall shaped as hyperbolic tangent with rise/fall time of 6 ns. The effective pulse width is the sum of the duration of the flat top pulse, half of the rise time and half of the fall time. Figure S2a shows the Rabi oscillations measured for an effective pulse width up to 220 ns, demonstrating Rabi amplitude of 0.996 ± 0.001. The calibration of the Rabi amplitude was done using separately measured maximum amplitude of the Rabi oscillations performed by a 20 ns Gaussian pulse with varying power. Figure S2b shows one of the slow Rabi flops whose decay time is 19 μs. Measured Rabi frequencies are ranged from 0.01 MHz to 100 MHz, as shown in Fig. S2c.

Fast single qubit gate operation and evaluation of the gate fidelity

To demonstrate fast single-qubit gate operation and to measure the gate fidelity, we performed the randomized benchmarking protocol first introduced by Knill et al. (9). We followed the identical procedure described in Ref. (10) where the benchmarking procedure was implemented to a superconducting qubit using optimized DRAG pulses (10) to minimize the leakage to the higher levels. Our single qubit gates are shaped with a Gaussian envelope truncated at 2σ at each end. Figure S3 shows the gate fidelity for a 20 ns gate (σ = 4ns). The fit to the data shows that the gate error is 2.5×10^{-3}.

Stability of relaxation time and coherence time

The relaxation time T_1 and the coherence time T_2 of qubit J1 were measured repeatedly for 23 hours. The coherence time T_2 is obtained from the same Ramsey experiments that yielded Δf_{01} shown in Fig. 3c in the main text.

Supplementary references

1. J. Majer et al. *Nature* **449** 443-447 (2007)
2. A. A. Houck et al. *Phys. Rev. Lett.* **101**, 080502 (2008)
3. L. DiCarlo et al. *Nature* **460**, 240-244 (2009)
4. J. M. Chow et al. *Phys. Rev. A.* **81**, 062325 (2010)
5. J. M. Chow et al. *Phys. Rev. A* **82**, 040305 (2010)

6. L. DiCarlo et al. *Nature* **467**, 574-578 (2010)
7. G. Catelani et al., *Phys. Rev. Lett.* **106**, 077002 (2011).
8. G. Catelani,et al. in preparation.
9. E. Knill et al. *Phys. Rev.* A 77, 012307 (2008)
10. J. M. Chow et al. *Phys. Rev.* A **82**, 040305(R) (2010)

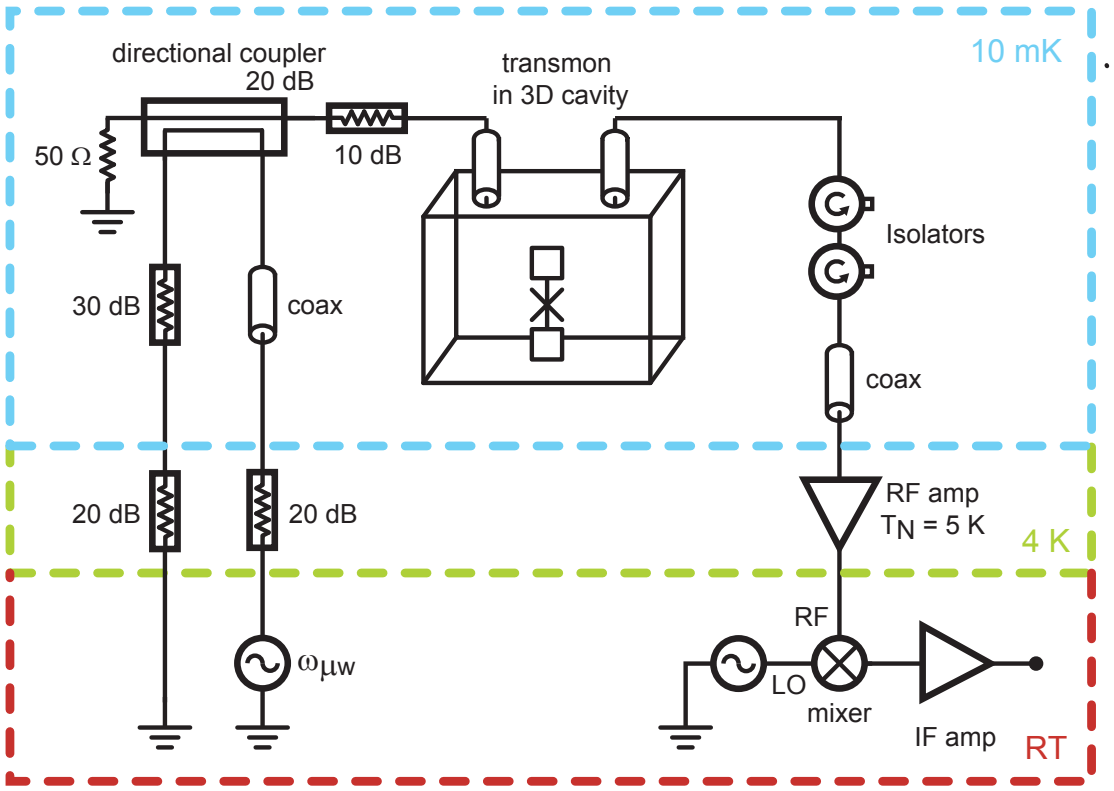

Fig. S1.
Block diagram of the measurement setup. Measurements were performed in a cryogen-free dilution fridge at 10 mK. Input signals are attenuated by a 20 dB attenuator at 4 K and a directional coupler (-20 dB) with a 10 dB attenuator at 10 mK.

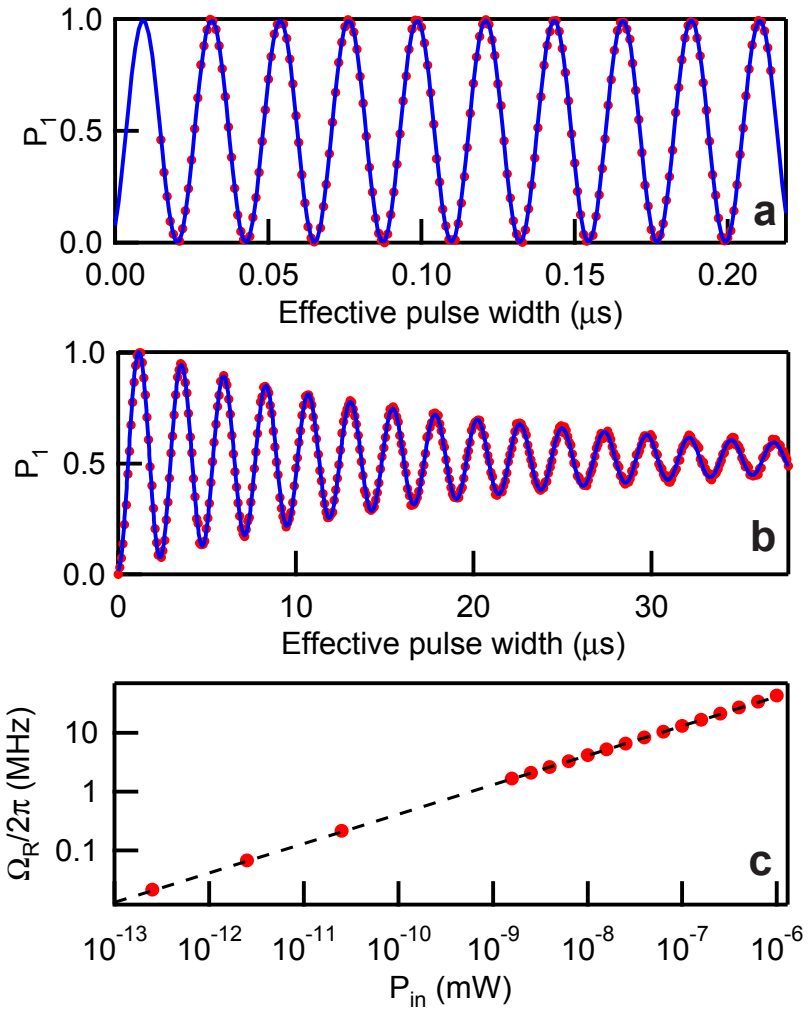

Fig. S2
Time domain Rabi oscillations from transmon J2 measured up to (a) 220 ns and (b) 38 μs. The red dots are the data and the blue curves are fit to the exponentially decaying sinusoidal function. The decay time of the oscillations shown in the graph is 19 μs. (c) Rabi frequency Ω_R vs. input power P_{in}. The dashed line is fit to the square root of the input power in milli-Watts.

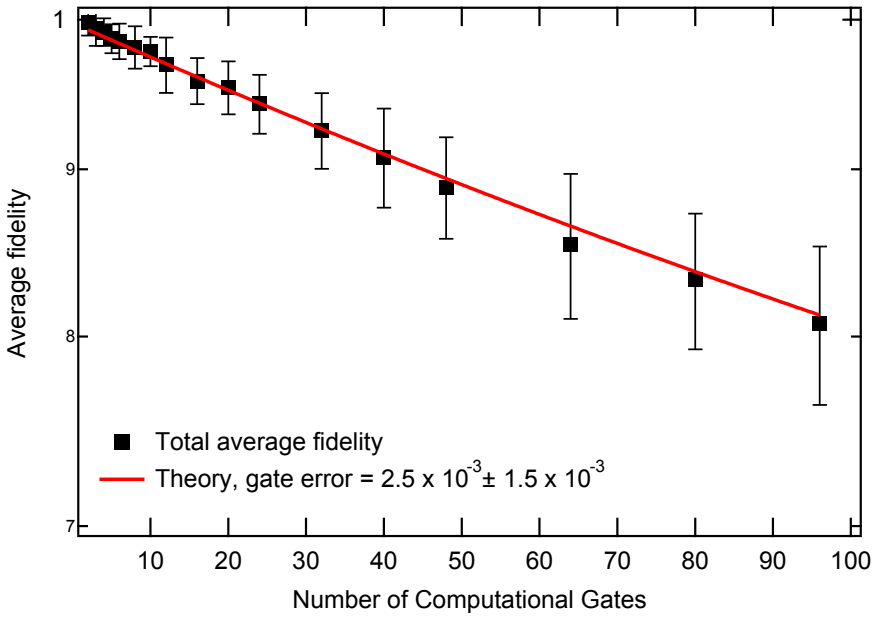

Fig. S3
Single qubit gate fidelity vs number of applied computational gates.obtained by a randomized benchmarking sequence. The data is measured with qubit *S*. The gate time is 20 ns.

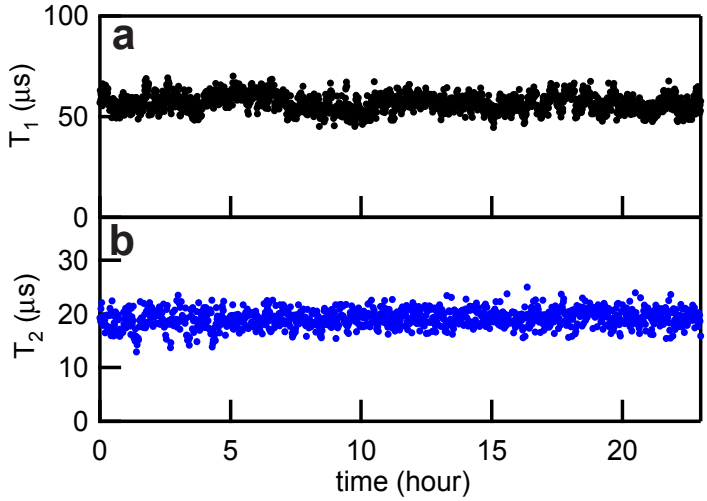

Fig. S4
Twenty-four hour repeated measurements of (a) T_1, (b) T_2 from qubit J1. The relaxation time T_1 shows random fluctuations with the standard deviation of 7 % and the coherence time T_2 with the standard deviation of 10 % from the the mean value. The data of T_1 and T_2 were measured separately but the data of T_2 were obtained from the same repeated Ramsey experiments where Δf_{01} data shown in Fig. 3c in the main text were obtained.